

ChemComm

Chemical Communications

Accepted Manuscript

This article can be cited before page numbers have been issued, to do this please use: G. Martínez, S. Delgado, A. Madrid, S. Díaz Coello, E. Pakrieva, M. C. Arevalo, E. Pastor, J. L. Hueso and J. Santamaria, *Chem. Commun.*, 2026, DOI: 10.1039/D5CC05420F.



This is an Accepted Manuscript, which has been through the Royal Society of Chemistry peer review process and has been accepted for publication.

Accepted Manuscripts are published online shortly after acceptance, before technical editing, formatting and proof reading. Using this free service, authors can make their results available to the community, in citable form, before we publish the edited article. We will replace this Accepted Manuscript with the edited and formatted Advance Article as soon as it is available.

You can find more information about Accepted Manuscripts in the [Information for Authors](#).

Please note that technical editing may introduce minor changes to the text and/or graphics, which may alter content. The journal's standard [Terms & Conditions](#) and the [Ethical guidelines](#) still apply. In no event shall the Royal Society of Chemistry be held responsible for any errors or omissions in this Accepted Manuscript or any consequences arising from the use of any information it contains.

COMMUNICATION

Received 00th January 20xx,
Accepted 00th January 20xx

DOI: 10.1039/x0xx00000x

Fe single-atom catalysts supported on N-enriched carbon promote the liquid phase electro-reduction of carbon dioxide to formic acidGema Martinez^{a,b,c,d,†}, Stefan Delgado^{e,†}, Ainhoa Madrid^{a,c}, Sergio Díaz-Coello^e, Ekaterina Pakrieva^{a,b,c}, María del Carmen Arévalo^e, Elena Pastor^{e,*}, Jose L. Hueso^{a,b,c,f,g,*}, Jesus Santamaría^{a,b,c,f}

This work describes how the presence of Fe single atom catalysts (Fe-SAC) dispersed on a nitrogen-enriched carbon matrix favours the selective electrocatalytic reduction of dissolved carbon dioxide to formic acid in neutral medium. Fe-SAC and Fe-free carbons were prepared by laser pyrolysis of phthalocyanine-pyridine aerosols.

Carbon dioxide conversion into added-value chemicals and fuels represents a formidable challenge towards a sustainable energy transition. Current innovation and research strategies include: (i) novel process intensification reactors with alternative activation strategies (i.e. photons, plasma, microwaves, electricity)¹⁻⁷ and (ii) the development of innovative materials able to maximize the interaction (adsorption-reaction) with CO₂. Regarding the latter, the use of atomically dispersed catalysts (also known as single-atom catalysts or SACs) emerges as one of the most promising strategies to achieve highly selective conversion of CO₂ while minimizing the use of expensive and scarce noble metals⁸⁻¹⁵. The combination of transition metal based SACs (i.e. Cu, Co, Fe) and electrocatalysis has yielded excellent results to obtain highly selective conversion of CO₂ into light hydrocarbons or alcohols, although there is still room to improve the interaction of dissolved CO₂ with the catalysts^{2, 16-20}. Some of the most successful SACs for CO₂ reduction are based on isolated atoms

dispersed in carbon matrices generally obtained by top-down thermal decomposition of preformed metal-organic frameworks (MOFs). This yields a high control on the catalyst structure key for some designs (e.g. dual-metal SACs) and benefits from the high conductivity of the carbon matrix obtained^{10, 21-24}. However, it also increases complexity, as it involves an additional synthesis step, and cost (the use of an expensive MOF material as a sacrificial matrix). In this work, we used a direct bottom-up approach based on the laser-driven pyrolysis of aerosols containing Fe-phthalocyanine (Fe-Ph) suspended in pyridine to obtain Fe-SACs supported within a carbon matrix (**Fig. 1a** and **Fig. S1**). The continuous wave infrared laser instantly decomposes the precursor droplets thereby trapping the isolated metals in a carbon matrix and minimizing nanoparticle nucleation and growth events during the decomposition process²⁵. In addition, a rapid quenching occurs out of the laser reaction zone (a temperature decrease of up to 150 degrees per mm)²⁶ also preventing migration and coalescence of atoms. We also synthesized Fe-free N-doped carbons under analogous reaction conditions with Fe-free Ph to yield N-enriched carbons (Fe-free N-Cs) (**Fig. S2**) and establish the influence of the Fe sites on the electrocatalytic reduction of CO₂ (ECO₂RR).

Figs. 1b-1d and **Fig. S1** show evidence of atomically dispersed Fe features in N-doped carbons. Additional evidence from EXAFS data was presented in previous works²⁴. The carbon particles hold an uneven size distribution and exhibit partial interconnection as previously observed in other particle morphologies synthesized by laser pyrolysis. The brighter contrast spots correspond to the presence of atomically dispersed Fe atoms with higher Z number. Overall, the EDX signal of Fe could only be detected after accumulation in broad areas (**Fig. S3**). Furthermore, N signal could be also detected for both the Fe-SACs and specially its Fe-free N-Cs counterpart (**Fig. S2c**). The N₂ adsorption-desorption isotherms showed a slight separation between the adsorption and desorption branches at higher relative pressures ($p/p^0 > 0.8$), suggesting the presence of mesopores but with only a minor hysteresis loop (**Fig. 1e** and **Fig. S2e**).

^a Instituto de Nanociencia y Materiales de Aragón (INMA) CSIC-Universidad de Zaragoza, Campus Rio Ebro, Edificio I+D, C/ Poeta Mariano Esquillor, s/n, 50018, Zaragoza, Spain. *Email: lhueso@unizar.es

^b Department of Chemical and Environmental Engineering, University of Zaragoza, Campus Rio Ebro, C/María de Luna, 3, 50018 Zaragoza, Spain.

^c Networking Research Center on Bioengineering, Biomaterials and Nanomedicine (CIBER-BBN), 28029, Madrid, Spain

^d Centro Universitario de la Defensa (CUD); Ctra. de Huesca 50090 Zaragoza, Spain

^e Instituto de Materiales y Nanotecnología, Departamento de Química, Universidad de La Laguna, Av. Astrofísico Francisco Sánchez s/n, 38206, San Cristóbal de La Laguna, España. * Email: epastor@ull.edu.es

^f Instituto de Investigación Sanitaria (IIS) de Aragón, Avenida San Juan Bosco, 13, 50009 Zaragoza, Spain

^g Escuela Politécnica Superior, U. Zaragoza, Ctra. de Cuarte s/n, 22071, Huesca, Spain.

† Equal contribution

Supplementary Information available: [Characterization techniques, additional figures and tables and experimental methods]. See DOI: 10.1039/x0xx00000x

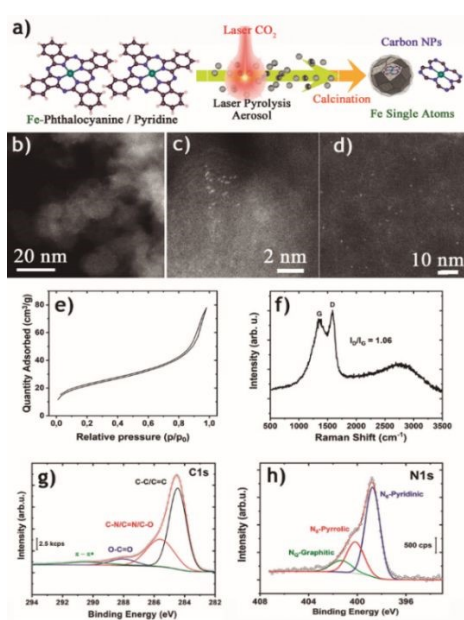


Fig. 1. Synthesis and characterization of Fe-SAC by laser pyrolysis: a) Simplified scheme of laser driven pyrolysis of Fe-phthalocyanine-pyridine aerosol droplets to yield Fe-SACs. b)-d) HAADF-STEM representative images of the Fe-SACs samples; e) N_2 adsorption isotherms at 77 K of the Fe-SACs; f) Representative Raman spectrum of the Fe-SACs; g) Fitted XPS of the C1s region; h) Fitted XPS of the N1s region.

Given the limited Fe content, partial pore blockage can be ruled out, and a change of chemical properties due to structural rearrangements caused by metal coordination seems a more likely cause. The pore size distributions, calculated using the non-local density functional theory (NLDFT) method, confirm that both materials possess pores within the mesoporous range (2-13 nm) (Fig. S4). The Fe-free N-Cs featured a broader mesoporous distribution, along with a total pore volume of $0.24 \text{ cm}^3/\text{g}$, whereas the Fe-SAC exhibited substantially lower porosity ($0.12 \text{ cm}^3/\text{g}$), indicating that the presence of Fe effectively produces a denser material (Table S1). Raman analysis confirmed the presence of both disordered and graphitic domains at $\sim 1350 \text{ cm}^{-1}$ and $\sim 1590 \text{ cm}^{-1}$, respectively (Fig. 1f and Fig. S2f). The higher I_D/I_G ratio for the Fe-SAC further suggested a higher disorder state induced by the presence of isolated Fe. X-ray photoelectron spectroscopy (XPS) revealed the surface composition for both samples with significant presence of C, N and O and trace signals of S or F (from SF_6 , employed as a sensitizer). Fe signal was barely detectable for Fe-SAC (Fig S5 and Table S2). Fitting of the C1s region revealed the presence of C-N/C-O species at B.E.s of 286.5 eV, O-C=O species at 287.9 eV and $\pi-\pi^*$ interactions at 290 eV, respectively (Fig. 1g and Fig. S2g). Likewise, the fitting of the N1s region²⁷ revealed the presence of pyridinic-N (B.E. = 398.3 eV), pyrrolic-N (400.1 eV), quaternary-N (401.5 eV) in both samples, along with the additional appearance of oxidized-N in the Fe-free N-C above 403 eV confirming the presence of N-enriched domains formed by laser pyrolysis (Fig. S1h). The catalytic response of Fe-SAC was evaluated towards the ECO_2RR in neutral medium (phosphate buffer solution; pH = 7.4) using Differential Electrochemical Mass Spectrometry (DEMS)²⁸ to

simultaneously monitor the Faradaic current and the ionic currents associated with the reaction products (see **Supplementary Note 1**, Fig. 2 and Figs. S6-S8). Briefly, the experiment was carried out in a three-electrode half-cell where a glassy carbon disk was modified with 20 μL of the catalytic ink and used as working electrode. The amount of ink was set to obtain a metallic load of 0.09 μg of Fe. The electrode was immersed at 0.2 V in a buffer phosphate solution (0.1 M Na_2HPO_4 / 0.1 M $NaH_2PO_4 \cdot 2H_2O$; pH = 7.5) saturated with CO_2 (99.998 %). Then, the surface potential was linearly swept towards cathodic values while recording both the faradaic current and the respective ionic currents (see the **Experimental Methods** in the ESI for further details). A control experiment in Ar ambient (in absence of CO_2) was also carried out for comparison. Fig. 2a shows that the saturation of the electrolyte with CO_2 increased the faradaic response during the cathodic polarization (linear sweep voltammetry, LSV) of the catalyst. In particular, the total current at -1.0 V increases from -0.8 mA to -1.5 mA, revealing the existence of an additional process corresponding to the ECO_2RR . This aligns well with the works reported by Varela et al.^{29, 30}. On the other hand, Figs. 2b-2c display the mass spectrometry signals (MSLSVs) corresponding to the evolution of hydrogen ($m/z = 2$) and formate ($m/z = 45$), respectively. While linking the $m/z = 2$ signal with the $[H_2]^+$ ion is straightforward, the correspondence of $m/z = 45$ with the $[HCOO]^+$ fragment from formate was established from the conditions of the experiment. **Supplementary Note 1** and Fig. S6 further explain about the most plausible product distribution and the species ruled out according to DEMS experiments. It is interesting to note that the responses for $m/z = 2$ were practically identical in the presence and absence of CO_2 beyond the onset overpotential (approx. -0.5 V) until -0.8 V, but then the production of H_2 was lower for the CO_2 saturated solution. This indicates that the hydrogen evolution reaction (HER) is partially blocked during the ECO_2RR (Scheme S1). No additional by-products associated with the ECO_2RR were identified by DEMS (e.g., methane monitored by the signal $m/z = 15$, Fig. S7b, or methanol by the mass $m/z = 31$, Fig. S8d). This is important since it contrasts with the high efficiency towards methane reported for other Fe-based materials³⁰.

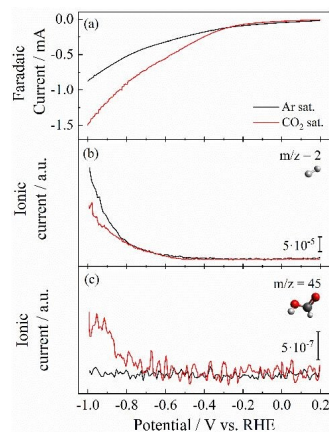


Fig. 2. LSVs (a) and the corresponding MSLSVs for $m/z = 2$ (b), $m/z = 45$ (c), recorded for Fe-SAC in 0.1 M phosphate buffer solution (pH = 7.5) at 2 mV/s, in Argon and CO_2 saturated solutions, respectively.

At -0.5 V the signal for $m/z = 45$ started being detected, revealing the formation of formate as the main product of the ECO_2RR process (**Fig. 2c**). Hence, the Fe-SAC: (i) preferentially produces formic acid during the ECO_2RR in neutral medium (**Scheme S1**); and (ii) does not lead to the formation of C_2 products. The faradaic efficiencies (FE) towards the HER have been estimated by comparing the ionic currents before and after CO_2 saturation of the electrolyte (see **Fig. S9**). As no other products besides H_2 and formate were detected in the potential range between -0.65 and -0.90 V vs. RHE, we assume that the difference between FE for H_2 in CO_2 -saturated conditions is due to the generation of formate. Thus, a FE of ~57 % at -0.90 V have been derived from the experiments. This agrees with the characteristics of SACs materials since each isolated Fe site acts as a center of reaction for the CO_2 molecule, sterically avoiding the C-C coupling of two different molecules¹⁸.

As shown in **Table S3**, analogous materials exhibit high selectivity towards the formation of CO due to the preferential adsorption of the CO_2 molecule to form the $^*\text{COOH}$ intermediate. In contrast, the laser pyrolysis method induces the generation of O-based functional groups, promoting instead the $^*\text{OHCO}$ adsorbate and formate formation (**Supplementary Note 2**). As specified in the latter, as well as in **Table S3**, the selectivity towards formate was linked not only to the material itself, but also to the usage of $\text{pH} = 5$ phosphate buffer as electrolyte for the reaction. Finally, an increase in the signals for $m/z = 32$ and $m/z = 28$ was observed but these ionic currents are not related to other products of the ECO_2RR (see discussion below). In addition to the formation of formate as the main product of the ECO_2RR , DEMS also provided information about the mechanism from the Tafel slopes for H_2 production (**Figure 3** and **Supplementary Note 3**). Indirectly, the evaluation of HER kinetics can shed light on the performance of the ECO_2RR since both reactions compete for the same active sites³¹⁻³³. Typically, Tafel slopes are derived from LSV experiments. However, if the polarization response during the experiment does not exclusively arise from the HER, Tafel slope values are overestimated, as can be seen in **Figure 3a**, with values that are clearly over the theoretical limit of $120 \text{ mV}\cdot\text{dec}^{-1}$ (364 and 627 mV dec^{-1} respectively in the presence and absence of CO_2). Instead, we have used the method previously reported by Diaz-Coello et al.^{28, 34}, in which the Tafel slopes are derived for the HER from the $m/z = 2$ ionic currents recorded during the DEMS experiments. In this method, the linear regression of the slopes was calculated from the onset potential of the reaction (easily readable at the $m/z = 2$ panel of the DEMS experiment) and extended for 50 – 100 mV of the cathodic scan (if linearity is maintained in this range). **Fig. S9** also marks the specific range used in this work, and **Supplementary Note 3** extends the information of the method and theory of the HER mechanism. **Figure 3b** shows that this approximation resulted in Tafel slopes inside the range theoretically accepted (from 30 to $120 \text{ mV}\cdot\text{dec}^{-1}$). In the Ar saturated solution, a Tafel slope of $79 \text{ mV}\cdot\text{dec}^{-1}$ was obtained, while in the CO_2 saturated electrolyte it shifted to $120 \text{ mV}\cdot\text{dec}^{-1}$. This implies a modification in the kinetics of HER. In the former reaction scenario, both the

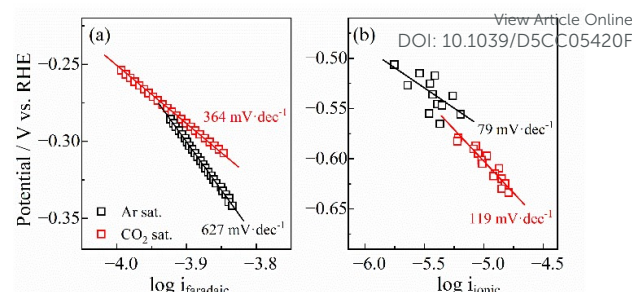


Fig. 3. Tafel plots derived from (a) faradaic currents and (b) $m/z = 2$ ionic currents recorded for Fe-SAC during the DEMS experiment shown in Figure 2.

Volmer and the Heyrovsky reactions are involved in the rate-determining step (RDS) of the whole process³⁴. Thus, some reaction sites are available to reduce water molecules, while others are kinetically hampered to facilitate the first reduction step of water^{32, 33}. In contrast, when the electrolyte is saturated with CO_2 , the Tafel slope showed a value of $120 \text{ mV}\cdot\text{dec}^{-1}$, which implies the Volmer reaction as sole RDS of the process. This behavior suggests that CO_2 occupies active surface sites, thereby hindering H adsorption and inhibiting the HER. This is well aligned with the DEMS experiment presented on **Fig. 2b**, where the generation of H_2 significantly decreases. Additionally, the stability of Fe-SAC was studied by chronoamperometry (CA)-DEMS in the potential range of the HER. **Fig. 4** shows an experiment carried out by recording the current transients at 0.2 V for 120 s, and then at -1.0 V for 300 s, respectively. Applying the latter potential to the material in the presence of CO_2 resulted in higher faradaic currents in comparison with the Ar saturated experiment (**Fig. 4a**) due to CO_2 electroreduction, confirming the results obtained in **Fig. 2a**. Furthermore, there was a significant inhibition in the formation of H_2 ($m/z = 2$, **Fig. 4b**) coupled with an enhanced formation of formate ($m/z = 45$, **Fig. 4d**) under CO_2 saturated conditions. This was also in agreement with the results presented in **Fig. 2b-c**. However, further screening of m/z from 15 to 32 values in DEMS experiments confirmed the sole presence of signals for $m/z = 32$ (**Fig. 4c**) and $m/z = 28$ (**Fig. S7c** and **S7f**) which led us to assign these mass ratios to $[\text{N}_2\text{H}_4]^+$ and $[\text{N}_2]^+$ fragments from the hydrazine molecule, respectively. The formation of hydrazine is obviously not arising from the reduction of CO_2 , but rather as a product of the Fe center environment degradation, that is, hydrazine is produced from the N atoms anchoring the Fe to the C network. In the absence of CO_2 , $m/z = 32$ (**Fig. 4c**, black line) increased after reaching -1.0 V and then it decreased over time, revealing the loss of active sites for hydrazine production under the applied potential. Remarkably, this process was accompanied by a decrease in the generation of H_2 (**Fig. 4b**, black line), which strengthens the hypothesis of the close correlation between both processes (**Scheme S2**). While hydrazine may hold certain safety concerns, in this study, our proposed degradation mechanism suggests the transformation of 1 mol of hydrazine per mol of Fe in the material (approx. $1.57 \cdot 10^{-6}$ mol of Fe on top of the working electrode). Assuming complete degradation of the material, which was not the case, the amount of hydrazine generated would not reach the safety



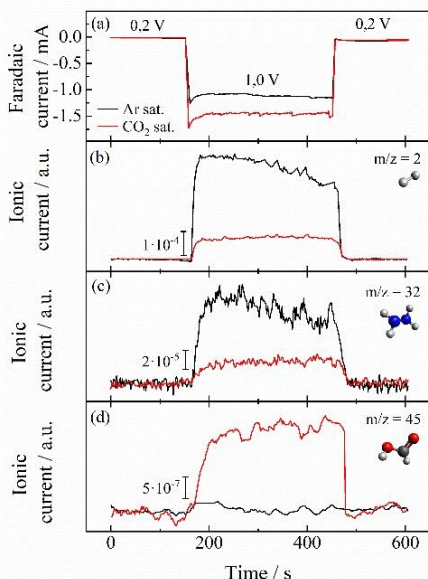


Fig. 4. a) CA carried out in the presence and absence of CO₂ and corresponding mass spectra for: b) m/z = 2, c) m/z = 32 and, d) m/z = 45 recorded over 10 minutes in 0.1 M phosphate buffer solution at pH 7.5

threshold. Remarkably, the DEMS experiment allowed the detection of this molecule, even at trace levels. Altogether, it seems reasonable that the hydrazine is formed by the hydrogenation of the N atoms in the Fe-based SAC due to the adsorption of H₂ at the Fe active centers (**Scheme S2**). However, this reaction was almost suppressed in the presence of dissolved CO₂ (**Fig. 4c**, red line) and the H adsorption step on the active site became the slowest process, and became impeded (**Fig. 4b**, red line), thereby increasing the stability and enabling the use of Fe-SAC for the ECO₂RR. To validate the specific influence of Fe to direct the selectivity towards hydrazine, we performed a control experiment with the Fe-free NCs (**Fig. S10**). This experiment was key to evaluate the behavior of the target material since no increase was found in m/z = 32 or 45 for the Fe-free carbon support. This demonstrated: (i) the catalytic activity of the metallic centers in the formation of formate; and (ii) the lack of formation of hydrazine in the absence of Fe. In both cases, the role of the Fe as reaction center was corroborated. This also confirmed that the active sites of the electrocatalyst are protected during the ECO₂RR. The stability towards the CO₂ reaction has also been tested (**Fig. S11**). The results show good stability under operating conditions for 1 hour with constant hydrogen and formate production. Remarkably, the same experiment in absence of CO₂ resulted in loss of activity caused by the degradation of the metallic center to form hydrazine after 45 min of applied potential (**Fig S11c**). This confirms both the intrinsic stability of the material for the ECO₂RR reaction as well as the proposed mechanism for the degradation of the Fe center. In addition, the FE of the products have been calculated in this chronoamperometric experiment, showing approximately the same values as the polarization experiments in **Fig. S9**, corroborating the previous result. Summarizing, this work demonstrates the active role of Fe-SAC synthesized by laser pyrolysis to selectively electro-generate formate from CO₂ thereby paving the way towards the design of novel electrocatalysts based on Fe-SAC.

Acknowledgements

View Article Online

DOI: 10.1039/D5CC05420F

The authors acknowledge funding from the Spanish Research Agency (AEI) through project CNS2022-135911 and Severo Ochoa: CEX2023-001286-S, Project PID2023-1507070B-I00, funded by MCIN/AEI/10.13039/501100011033, and the ULL-Cabildo de Tenerife-TALENTUM program. The synthesis of materials has been performed by the Platform of Production of Biomaterials and Nanoparticles of the NANBIOSIS ICTS, more specifically by the Nanoparticle Synthesis Unit (Unit 9) of the CIBER in Bioengineering, Biomaterials & Nanomedicine (CIBER-BBN). The authors acknowledge the use of instrumentation and technical support provided by the National Facility ELECMII ICTS, node 'Laboratorio de Microscopías Avanzadas (LMA)' at the Universidad de Zaragoza. S.D. thanks ACIISI (Agencia Canaria de Investigación, Innovación y Sociedad de la Información) and the European Social Fund (ESF) (Operative Integrated Program of Canary Islands Integrated Operational Program 2021–2027, Area 3 Priority Theme 74 (85%)) for his predoctoral contract (TESIS2022010136). S.D.-C. acknowledges the ULL-Cabildo de Tenerife-TALENTUM program for the postdoctoral contract. E.P. thanks Juan de la Cierva Formación postdoctoral fellowship (JDC2022-049007-I) financed by MICIU/AEI/10.13039/501100011033 and by the European Union "NextGenerationEU"/PRTR".

Conflicts of interest

There are no conflicts to declare.

Data availability

The data supporting this article have been included as part of the Supplementary Information.

Notes and references

- Y. Hori, K. Kikuchi and S. Suzuki, *Chemistry Letters*, 1985, **14**, 1695-1698.
- S. Back, J. Lim, N.-Y. Kim, Y.-H. Kim and Y. Jung, *Chemical Science*, 2017, **8**, 1090-1096.
- S. Nitopi, E. Bertheussen, S. B. Scott, X. Liu, A. K. Engstfeld, S. Horch, B. Seger, I. E. L. Stephens, K. Chan, C. Hahn, J. K. Nørskov, T. F. Jaramillo and I. Chorkendorff, *Chemical Reviews*, 2019, **119**, 7610-7672.
- A. I. Stankiewicz and H. Nigar, *Reaction Chemistry & Engineering*, 2020, **5**, 1005-1016.
- J. L. Hueso, R. Mallada and J. Santamaria, *Catalysis Today*, 2023, **423**, 113927.
- C. Faria, C. Rocha, C. Miguel, A. Rodrigues and L. M. Madeira, *Fuel*, 2025, **386**, 134269.
- K. M. Van Geem, V. V. Galvita and G. B. Marin, *Science*, 2019, **364**, 734-735.
- Y. Cai, J. Fu, Y. Zhou, Y.-C. Chang, Q. Min, J.-J. Zhu, Y. Lin and W. Zhu, *Nature Communications*, 2021, **12**, 586.
- X. Kang, L. Li, A. Sheveleva, X. Han, J. Li, L. Liu, F. Tuna, E. J. L. McInnes, B. Han, S. Yang and M. Schröder, *Nature Communications*, 2020, **11**, 5464.
- B. Peng, H. She, Z. Wei, Z. Sun, Z. Deng, Z. Sun and W. Chen, *Nature Communications*, 2025, **16**, 2217.

Journal Name

COMMUNICATION

11. N. Wang, W. Jiang, J. Yang, H. Feng, Y. Zheng, S. Wang, B. Li, J. Z. X. Heng, W. C. Ong, H. R. Tan, Y.-W. Zhang, D. Wang, E. Ye and Z. Li, *Nature Communications*, 2024, **15**, 5913.

12. Q. Wang, T. Luo, X. Cao, Y. Gong, Y. Liu, Y. Xiao, H. Li, F. Gröbmeyer, Y.-R. Lu, T.-S. Chan, C. Ma, K. Liu, J. Fu, S. Zhang, C. Liu, Z. Lin, L. Chai, E. Cortes and M. Liu, *Nature Communications*, 2025, **16**, 2985.

13. C. Zhan, F. Dattila, C. Rettenmaier, A. Herzog, M. Herran, T. Wagner, F. Scholten, A. Bergmann, N. López and B. Roldan Cuenya, *Nature Energy*, 2024, **9**, 1485-1496.

14. R. I. Masel, Z. Liu, H. Yang, J. J. Kaczur, D. Carrillo, S. Ren, D. Salvatore and C. P. Berlinguette, *Nature Nanotechnology*, 2021, **16**, 118-128.

15. N. Ye, K. Wang, Y. Tan, Z. Qian, H. Guo, C. Shang, Z. Lin, Q. Huang, Y. Liu, L. Li, Y. Gu, Y. Han, C. Zhou, M. Luo and S. Guo, *Nature Synthesis*, 2025, DOI: 10.1038/s44160-025-00769-9.

16. J. Gu, C. S. Hsu, L. C. Bai, H. M. Chen and X. L. Hu, *Science*, 2019, **364**, 1091-1094.

17. Z. Shang, X. T. Feng, G. Z. Chen, R. Qin and Y. H. Han, *Small*, 2023, **19**, 2304975.

18. L. Z. Liu, M. T. Li, F. Chen and H. W. Huang, *Small Structures*, 2023, **4**, 2200188.

19. J. Zhang, W. Cai, F. X. Hu, H. Yang and B. Liu, *Chemical Science*, 2021, **12**, 6800-6819.

20. L. H. A. Wijewardena, W. S. Cheon, S.-H. Jeong, J. Park and H. W. Jang, *RSC Sustainability*, 2025, **3**, 2779-2805.

21. W. Chen, B. Ma and R. Zou, *Accounts of Materials Research*, 2025, **6**, 210-220.

22. Z. Bai, Z. Zhi, X. Z. Jiang and K. H. Luo, *Industrial & Engineering Chemistry Research*, 2025, **64**, 4378-4387.

23. H. Huang, K. Shen, F. Chen and Y. Li, *ACS Catalysis*, 2020, **10**, 6579-6586.

24. M. Urso, X. Ju, R. Nittoor-Veedu, H. Lee, D. Zaoralová, M. Otyepka and M. Pumera, *ACS Catalysis*, 2025, DOI: 10.1021/acscatal.4c08027, 11617-11663.

25. A. Madrid, A. Tolosana-Moranchel, A. García, S. Rojas, F. Bartolome, E. Pakrieva, L. Simonelli, G. Martinez, J. L. Hueso and J. Santamaría, *Chemical Engineering Journal*, 2024, **498**, 155363.

26. A. Malumbres, G. Martinez, R. Mallada, J. L. Hueso, O. Bomati-Miguel and J. Santamaría, *Nanotechnology*, 2013, **24**, 325603.

27. J. L. Hueso, J. P. Espinós, A. Caballero, J. Cotrino and A. R. González-Elipe, *Carbon*, 2007, **45**, 89-96.

28. S. Díaz-Coello, G. García, M. C. Arévalo and E. Pastor, *International Journal of Hydrogen Energy*, 2019, **44**, 12576-12582.

29. A. S. Varela, M. Kroschel, N. D. Leonard, W. Ju, J. Steinberg, A. Bagger, J. Rossmeisl and P. Strasser, *ACS Energy Letters*, 2018, **3**, 812-817.

30. A. S. Varela, N. R. Sahraie, J. Steinberg, W. Ju, H. S. Oh and P. Strasser, *Angewandte Chemie-International Edition*, 2015, **54**, 10758-10762.

31. M. Khalil, G. T. M. Kadja, F. A. A. Nugroho, L. G. Sutanto, P. K. Jiwanti, F. F. Abdi, F. Hussin and M. K. Aroua, *Renewable & Sustainable Energy Reviews*, 2024, **206**, 114869.

32. L. Wang, X. K. Liu, L. L. Cao, W. Zhang, T. Chen, Y. Lin, H. J. Wang, Y. Wang and T. Yao, *Journal of Physical Chemistry Letters*, 2020, **11**, 6691-6696.

33. X. Wang, Y. Pan, H. Ning, H. Wang, D. Guo, W. Wang, Z. Yang, Q. Zhao, B. Zhang, L. Zheng, [View Article Online](#) [DOI: 10.1038/s44160-025-00769-9](#), *Applied Catalysis B: Environmental*, 2020, **266**, 118630.

34. S. Díaz-Coello, D. Winkler, C. Griesser, T. Moser, J. L. Rodríguez, J. Kunze-Liebhäuser, G. García and E. Pastor, *ACS Applied Materials & Interfaces*, 2024, **16**, 21877-21884.

Data availability statement

[View Article Online](#)
DOI: 10.1039/D5CC05420F

The data supporting this article have been included as part of the Supplementary Information.